

## On the dynamical evolution of Scattered Disk Objects outside the planetary system

R. Gabryszewski<sup>1</sup> and H. Rickman<sup>1,2</sup>

<sup>1</sup>Space Research Centre Polish Academy of Sciences,  
ul. Bartycka 18 A, 00-716 Warszawa, Poland  
e-mail: r.gabryszewski@cbk.waw.pl

<sup>2</sup>Department of Physics and Astronomy, Uppsala University,  
Box 515, Regementsvägen 1, SE-75120 Uppsala, Sweden

*Received July 12th, 2010*

### ABSTRACT

We report the results of dynamical simulations, covering Gyr timescales, of fictitious Scattered Disk Objects as a follow-up to an earlier study by Fernández et al. (2004: *Icarus* **172**, 372). Our dynamical model is similar in that it does not include external agents like passing stars or the Galactic tide. Only the four giant planets are explicitly treated as perturbers. We analyze the random-walk behavior of the inverse semi-major axis by means of a simplified circular restricted 3-body problem as an approximate analogue. Our results concerning the role of resonant effects and the transfer efficiency into the orbital energy domain of the inner Oort Cloud are in broad agreement with the earlier papers, and we confirm the important role of external objects (with perihelia beyond Neptune's orbit) in feeding the Oort Cloud. We estimate the efficiency of this transfer to be even somewhat higher than previously found.

**Key words:** *non-resonant dynamics, Oort Cloud objects, SDO, celestial mechanics, numerical integration*

### 1. Introduction

The Scattered Disk is one of the dynamical structures identified among Trans-Neptunian Objects (TNOs). Its existence was confirmed by the first discoveries in the mid-nineties (Luu et al. 1997). The bodies of this type are generally defined by the range of perihelion distances and/or semi-major axes ( $30 < q < 40$  AU,  $a > 50$  AU). Scattered Disk Objects (SDOs) can be perceived as TNOs that have evolved due to perturbations at close encounters with Neptune (Duncan & Levison 1997, Morbidelli & Brown 2004). These bodies seem to be an important link between TNOs and Oort Cloud comets (Fernández et al. 2004, Rickman et al. 2004).

The dynamical evolution of SDOs is also influenced by mean motion and Kozai resonances (Gomes et al. 2005, Gallardo 2006). According to these papers, objects

with eccentricities  $e < 0.9$  may experience temporary captures into mean motion resonances (MMRs). Most of these are of  $1/N$  type with respect to Neptune, acting on Myr timescales, but occasionally Gyr timescales have been observed too. The Kozai resonance is often found to act on bodies in MMR with inclinations higher than that of Pluto. Due to oscillations in the  $(e, i)$  plane coupled to  $\omega$  libration, this is a mechanism of changing the perihelion distance. Such changes may become permanent, if the body escapes from the resonance during a different phase of the cycle than where it entered.

This work presents the specific dynamics of non-resonant SDOs with large and quasi-constant perihelion distances outside the planetary system. Such bodies may experience large increases of semi-major axis and eccentricity on timescales much shorter than the age of the Solar System. We have analyzed the influence of orbital energy ( $1/a$ ) perturbations by Neptune and other giant planets on such objects, stimulated by the work of Fernández et al. (2004). Some remarks on the statistics of feeding the inner Oort Cloud region and the influence of resonances on SDO dynamics are also presented.

## 2. Numerical model

We use a sample of 100 test particles (TPs) on SDO-like orbits. The orbits are placed on a regular grid in  $(a, q, i)$  space ( $i$  is the inclination), as listed in Table 1. The TPs cover all the grid points, and for each one we define the initial condition at the beginning of the integration by considering in addition a value of  $\omega$  (argument of perihelion) that alternates between 90 and 270 degrees, and random values of  $\Omega$  (longitude of the ascending node) and  $M_o$  (mean anomaly at time zero). All the elements refer to the heliocentric frame. This remark is of special significance concerning the perihelion distances. While the pericenter distance of the barycentric orbit is relatively stable for high-eccentricity objects like the ones we consider, that of the heliocentric orbit is not. The velocity offset between the Sun and the barycenter will easily lead to relative changes of the perihelion distance by up to  $\pm 8\%$ . Thus, the actual perihelion distances, which apply when the objects pass perihelion, may be quite different from the ones listed in the Table.

The initial conditions for perihelion distances, semi-major axes and inclinations were chosen to cover the ranges occupied by most observed SDOs, up to nearly 10 AU outside Neptune's orbit, and some Neptune-crossers as well. We also considered the dynamics of some particles with much lower starting inclinations (0 to 0.1 degrees) as a test case. The results of these additional integrations are not included in statistics presented in Section 3.3, but one of the objects forms the basis for the discussion in Sect. 3.1.

The equations of motion were integrated numerically using a hybrid method from the MERCURY 6 package (Chambers 1999). This integrator is not fully symplectic. The MVS algorithm used in the symplectic part cannot handle close en-

Table 1

Values of heliocentric orbital elements characterizing the initial conditions of test particles.

$a$ (AU)	$q$ (AU)	$i$ (deg.)
100, 200, 500, 1000	28, 30, 32, 34, 36	10, 12.5, 15, 17.5, 20

counters, hence the Bulirsch-Stoer routine is used for integrating those approaches. The changeover distance was set to 3 Hill radii of the planet.

The equations of motion were those of the  $N$ -body problem with the Sun, four giant planets and test particles. Galactic tides were not included into our Solar System model. The integration time step used by symplectic routines was set to  $\sim 80$  days. The masses of terrestrial planets were added to the mass of the Sun, and the TPs were assumed to be massless. The objects were integrated over a maximum time of 2 Gyrs, but the integrations were finished earlier, when one of the following conditions occurred: (a) collision with a planet, (b) eccentricity greater than 0.9995, (c) semi-major axis greater than 25000 AU.

Various numerical tests were made before and during the integrations. Mainly, we inspected the outputs, comparing results from different methods of integration. But verification was made at nearly every step of the calculations.

Besides MERCURY 6 we used the RMVS3 symplectic integrator from the SWIFT package (Duncan & Levison 1997) and the recurrent power series (RPS) method introduced by Sitarski (2002). We examined the agreement between slowly varying orbital elements of test particles using all these methods until the first close planetary encounter. Thus, for objects without close approaches to the planets, we were able to verify that similar evolutions result on a time scale of 100 Myr. Moreover, in one case where the perihelion of the test particle remained more than 7.5 AU beyond Neptune's orbit (to be referred to below as TP LI), we got very similar evolutions using our standard method and the RPS method of integration during close to 1 Gyr. This was part of a check, where we compared the variations of  $1/a$  of randomly chosen test particles as calculated by the RPS method with the results from the MERCURY 6 package. The observed general dependencies were indeed of the same type (see Fig. 1).

Analysis of  $1/a$  perturbations was performed using the circular restricted 3-body problem (CR3BP) as a simple model. A dedicated program written by Hans Rickman was used to calculate the perturbations  $\Delta(1/a)$  experienced by an object on an unperturbed, parabolic orbit during one perihelion passage. This method allows to estimate the orbital energy change in the absence of close encounters for high eccentric SDOs evolving outside the planetary system with reasonable accuracy using very little computer time.

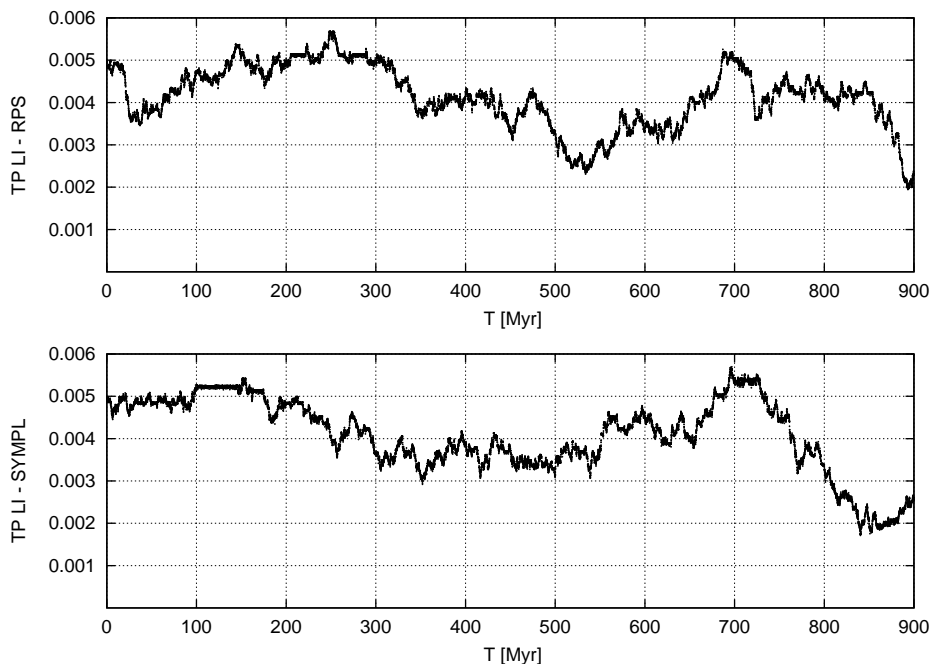


Fig. 1. Evolutions of orbital energy  $1/a$  (the inverse semi-major axis) as a function of time for the test particle TP LI. The lower graph shows the evolution obtained by the symplectic integrator used in our calculations. The upper graph presents the same evolution obtained by the RPS integrator. The changes of orbital energies are seen to follow similar patterns in both cases. The unit for  $1/a$  is  $\text{AU}^{-1}$ .

### 3. Results

#### 3.1. Non-resonant dynamics outside the planetary system

Planetary perturbations acting on SDOs usually cause random variations of non-angular orbital parameters. This pattern can change, if the geometry of encounters is repeating on a longer time scale, but in the absence of such resonant behavior, the variations of eccentricity and semi-major axis are generally accidental, and the long-term evolution can be described as a random walk.

In Fig. 2 we show a few typical examples of the evolution of orbital energy as measured by  $1/a$  (the inverse semi-major axis), illustrating what was said above. We see rather different behaviors in spite of the common random-walk picture, for various reasons. The case of TP 89 illustrates the behavior of particles moving into the inner core of the Oort Cloud with orbital periods hundreds of times larger than in the inner part of the scattered disk. Eventually, at  $T \simeq 1400$  Myr, this one is ejected from the Solar System. Other evolutions in the lower plots would look as flat, if their time axes were expanded by nearly a factor 100.

The case of TP 25 is interesting too, and now the relative flatness of the curve is explained by quasi-resonant dynamics. There are many MMRs, as is typical for such small semi-major axes, and a few are quite long-lasting ( $\sim 100$  Myr). We

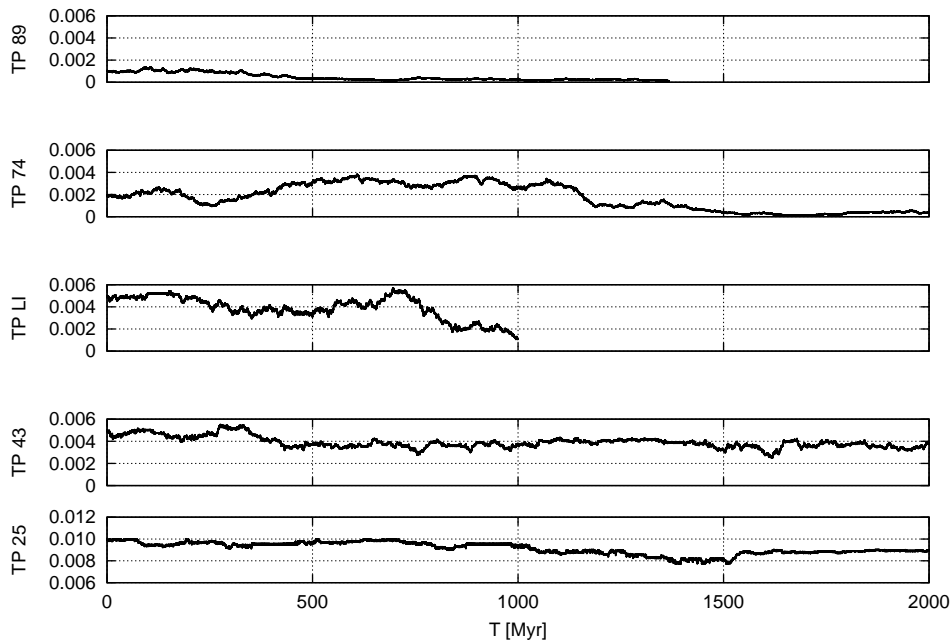


Fig. 2. Evolutions of orbital energies  $1/a$  (the inverse semi-major axis) as a function of time for five different test particles: TP 25, TP 43, TP LI, TP 74 and TP 89. TP LI is the particle from the test case set of initial conditions with low inclinations. It has the largest variations of  $1/a$  parameter of all the bodies with quasi-constant perihelion distance. The units for  $1/a$  is  $\text{AU}^{-1}$ .

have also included one of the low-inclination cases, for which the integration was limited to 1 Gyr. Particle TP LI exhibits the typical random-walk behavior at first glance, but near the end there is an extended period, during which there is an almost steady decrease of  $1/a$  ( $T \simeq 740 - 840$  Myr). Figure 3 shows some details of the dynamics of this particle.

The object is well separated from the planetary system. At perihelion it is close to 8 AU from Neptune's orbit, and this situation persists for the whole length of the integration. The change in semi-major axis between 740 and 840 Myr is seen to extend from 200 to 600 AU. There is no corresponding change in the behavior of the peribaryon distance, which remains almost constant. Instead we see a correlated, increasing trend in the eccentricity.

One interesting feature is that the variation of the argument of periapsis is distinctly slower compared to other time intervals – the value remains between  $-90$  and  $+90$  degrees. Such a slow  $\omega$  variation (if related to the trend in semi-major axis) may suggest that the limited range of  $\omega$  leads to a trend in the geometry of Neptune encounters close to the perihelion passages. We will discuss a possible effect of this kind below, but we note that any  $\omega$  effect must be severely limited in the present case by the smallness of  $i$ . We also investigated whether there is any repeatability of the angular distance between Sun-object and Sun-planet directions

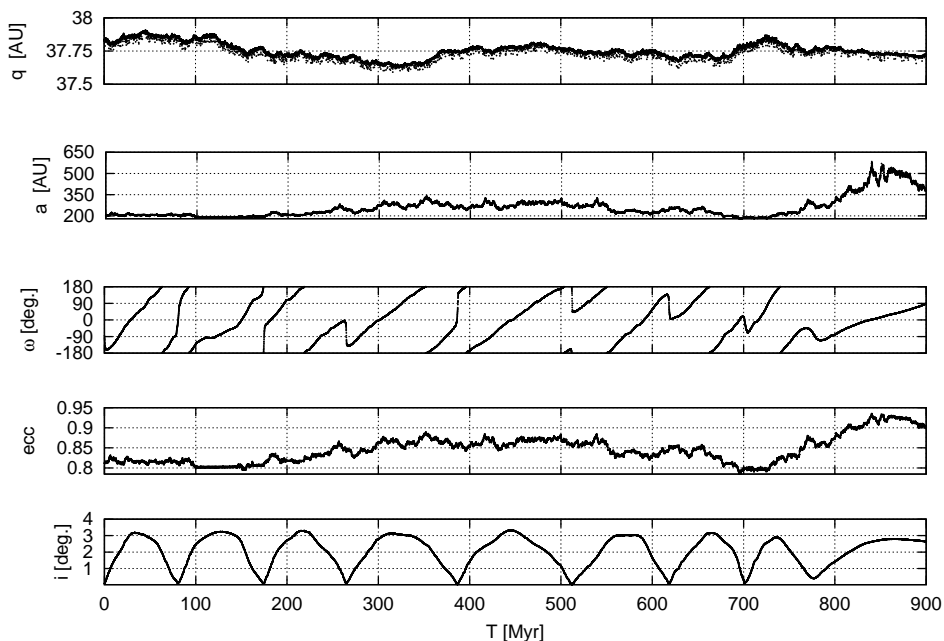


Fig. 3. Evolutions of five barycentric elements as functions of time. Particle TP LI was started with an inclination of 0.1 degree, a semi-major axis of 200 AU, and a perihelion distance close to 38 AU. Note that the quantity plotted here is the peribaryon distance, i.e., the pericenter distance of the osculating barycentric orbit. A major increase of the semi-major axis starts at  $T \sim 740$  Myr and continues for  $\sim 100$  Myr.

when the object passes perihelion, even though the rapidly varying semi-major axis effectively prevents any long-lasting effect of this kind. Indeed, no geometric repeatability was observed.

Some insight into this kind of dynamics can be obtained using a CR3BP model in which the small body moves on an unperturbed parabolic orbit. A procedure for computing such ‘Keplerian estimates’ of the energy perturbations  $\Delta(1/a)$  has been described by Rickman (2010), and we follow it here, using Neptune as the perturbing planet placed at 30.1 AU from the Sun. The test object has a perihelion distance of 38 AU, thus excluding the risk of close encounters and lending support to the approximation of an unperturbed orbit.

The integrations were done in the heliocentric frame, but we considered only the direct part of the perturbing function, so we actually compute the barycentric energy changes. Given the values of perihelion distance, inclination and argument of perihelion, only one more orbital parameter is needed, and we take this to be the angular distance between the projected Sun-object and Sun-planet lines at the time of the object’s perihelion passage. Let us call this angle  $\phi$ . The closest encounters will occur near  $\phi = 0$ . In this case the conjunction occurs near perihelion. Before conjunction the planet is ahead of the object, thus accelerating it, and after conjunction the reverse happens. Generally, for conjunction before perihelion,

there is hence a net deceleration, and for conjunction after perihelion there is a net acceleration. This will be seen as maximum positive and negative values of  $\Delta(1/a)$  occurring at either side of  $\phi = 0$ . In case  $\omega = 0$ , the object's perihelion point is practically in the planet's orbital plane, and the situation is symmetric so that the maximum positive and negative  $\Delta(1/a)$  have the same absolute value. But if  $\omega \neq 0$ , the symmetry is destroyed, and we get a predominance of either positive or negative  $\Delta(1/a)$ , depending on the sign of  $\omega$ . This effect will vanish for  $i = 0$  and increase in amplitude, when  $i$  takes larger values.

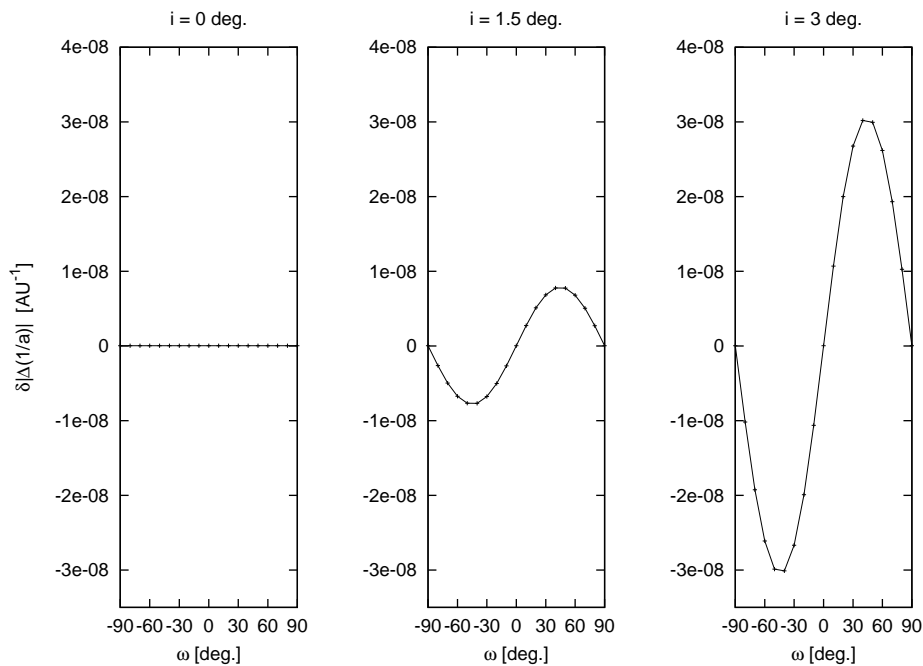


Fig. 4. Variations of differential  $1/a$  perturbations as a function of the argument of periapsis. The  $\delta|\Delta(1/a)|$  quantity is the difference between the absolute values of the largest positive and negative perturbations, considering all values of the planetary longitude at the time of perihelion passage of the object. The three panels give results for inclinations of 0, 1.5 and 3 degrees. See the text for details.

Figure 4 shows graphs of the difference between the absolute values of maximum positive and negative  $1/a$  perturbations vs  $\omega$  for inclinations similar to the particle under consideration. In Fig. 5 we show plots of the corresponding mean values of  $\Delta(1/a)$ , taken over all values of  $\phi$ . When the inclination is zero, as expected, the net differential or average effect is zero for all values of  $\omega$ . But when even a small inclination is set, the differential or average  $1/a$  perturbation starts to change in dependence of  $\omega$ . The largest values occur for inclinations close to 40 degrees and arguments of periapsis in ranges between 30 and 40 degrees in absolute value. However, they are far too small to have any effect in the long run, and even if they had, we would see opposite trends in  $1/a$  depending on the sign

of  $\omega$ , in conflict with what we observe in Fig. 3.

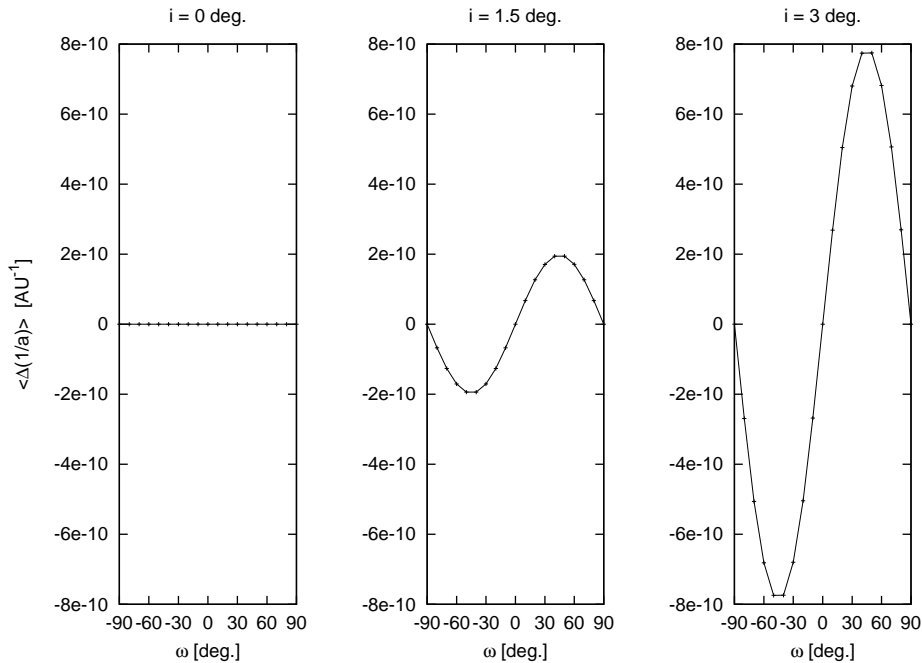


Fig. 5. Variations of mean value of  $\Delta(1/a)$  perturbations taken over all values of the  $\phi$  angle, as a function of argument of periastris. The three panels show results for inclinations of 0, 1.5 and 3 degrees. Note the different scale for this quantity compared to Fig. 4.

In quantitative terms, we observe in Fig. 5 that the average perturbation does not exceed  $10^{-9} \text{ AU}^{-1}$  in absolute value for any  $\omega$ . A time scale of 100 Myr corresponds to  $\sim 50000$  orbital revolutions, and thus, even if  $\omega$  would be locked at the optimum value for this period of time, the cumulative perturbation would be less than  $5 \cdot 10^{-5} \text{ AU}^{-1}$ , while the change observed in Fig. 3 is about 0.003 in the same units. On the other hand, the general level of the  $1/a$  perturbation at an arbitrary value of  $\phi$  is  $\sim 1 \cdot 10^{-5} \text{ AU}^{-1}$ , so a random walk with 50000 steps typically covers a range of 0.002 in rough agreement with what we see in the Figure.

Note, however, that high-inclination objects stand a better chance of being influenced by the considered differential effect. Close to  $i = 40^\circ$  we find average perturbations reaching close to  $10^{-7} \text{ AU}^{-1}$  in some ranges of  $\omega$ . Thus, if  $\omega$  circulates very slowly, significant evolution of  $1/a$  may in fact occur at such high inclinations.

### 3.2. Resonances and quasi-resonant states

During their evolution SDOs can experience temporary captures into two types of resonance: mean motion (MMR) and Kozai type. Due to the weak planetary perturbations outside Neptune's orbit, high-order MMRs may have a significant influence of SDO dynamics. This observation is in agreement with the conclusions



of Gomes and Gallardo, but there are also some differences.

In our results the maximum time intervals of single resonant states are up to  $\sim 100$  Myr and most often they are close to 20–30 Myr. This means the timescales are generally shorter than Gomes' results, but this difference may be caused by distinctions of the considered orbital populations. MMRs of  $2/N$  type were as frequently observed as  $1/N$  type. MMRs of  $3/N$  type were noticed only for SDOs evolving toward small semi-major axes. The time intervals of this latter resonant type were much shorter than in the other mentioned cases. All long lasting resonant states occurred with Neptune, and no stable MMRs were observed with any other planet.

Kozai cycles were observed in the simulations far less frequently than MMRs. We noticed only three of these. The longest capture lasted 400 Myrs (see Fig. 6), and none of them were coupled with any MMR. In all cases the change of perihelion distance was in the range of 2 AU or smaller, which is to be expected since we do not consider any very high inclinations. We did not observe the interruption of any Kozai cycle in a different phase than the one where it was entered. It seems that when the Kozai resonance is not associated to a MMR, there is no mechanism able to interrupt it in such a way as to trigger a large change in perihelion distance. This suggests that the Kozai resonance as a mechanism of perihelion distance increase need not be very efficient.

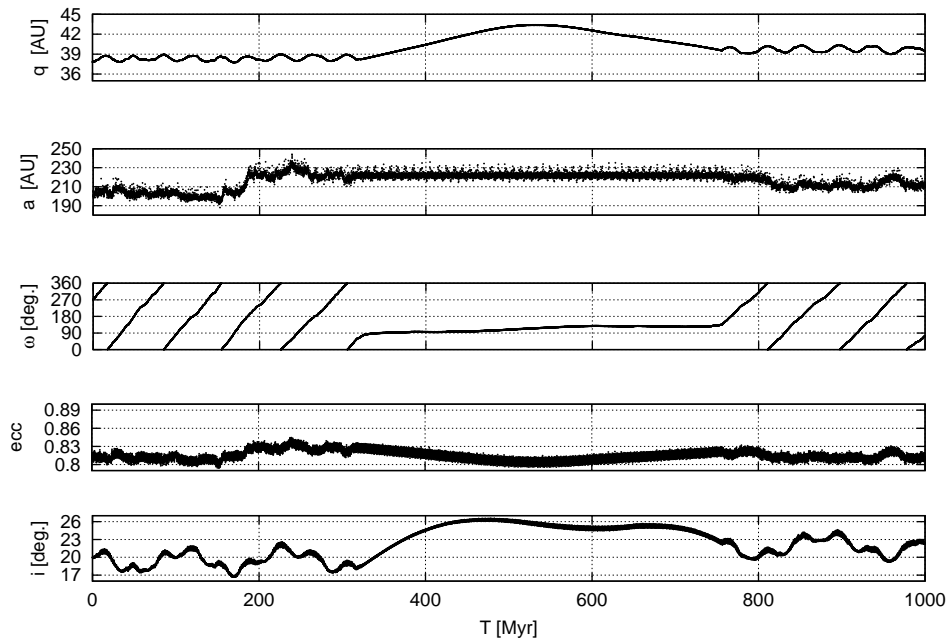


Fig. 6. TP 50: Dynamics of a body under the influence of the Kozai resonance. Its action changes the perihelion distance by only about 2 AU.

### 3.3. Oort Cloud transfers

The simulations allowed us to estimate how many SDOs may reach the inner Oort Cloud within the given time. Figure 7 shows the cumulative distribution of maximum semi-major axes for our 100 objects sample. Most SDOs evolve into the range of  $1000 < a < 10000$  AU, but the number of objects breaking the 10000 AU limit is much lower. If we assume an inner Oort Cloud limit at 5000 AU, the fraction of objects entering this region is 70%. If the limit is set to 10000 AU, the fraction of evolving objects decreases to 45%.

These results were obtained by counting the number of objects with semi-major axes taking values larger than the limit. The temporary acceleration and deceleration of an object encountering Neptune to within three Hill radii may cause rapid changes of  $1/a$  that are very important for highly eccentric SDOs like those we are investigating. Thus we might register very large values of the semi-major axis of a SDO close to the moment of its perihelion passage, when a close approach might occur. To avoid such errors, the condition if the semi-major axis surpasses the given limit was verified at true anomalies of more than  $1^\circ$  after perihelion when changes of the semi-major axis in subsequent data dumps were always  $< 5$  AU.

Our obtained numbers, quoted above, are in a good agreement with the outcomes of Fernández et al. (2004), who used a different condition, namely, the penetration of the object beyond  $r = 20000$  AU in heliocentric distance. The difference in fractions of objects reaching an inner Oort Cloud starting at  $a = 10000$  AU is only about 5%. Note, however, that the timescales of the two investigations are different: 2 Gyr in our case, and 5 Gyr for Fernández et al. (2004). We can therefore expect that our percentage would become a bit larger than that of Fernández et al. (2004), if we had integrated over as long a timescale as they did. Nonetheless, the difference is remarkably small, noting the large variations of initial conditions. The population used by Fernández et al. (2004) is based on 76 observed bodies with inclusion of their clones, while in this work we used a distribution of arbitrarily chosen initial conditions. Additionally, half of these objects had much larger values of initial semi-major axes (500 and 1000 AU), comparing to the population used by Fernández et al. (2004).

Let us note that limit of  $a = 10000$  AU is rather conservatively estimated. Many authors, like Duncan et al. (1987), advocate a closer limit for external agents to remove the perihelia – closer to the above number of 5000 AU. Thus we may estimate that a large majority of our treated SDOs will actually become potential inner Oort Cloud bodies on a 2 Gyr timescale.

While the fraction of SDOs entering inner Oort Cloud is thus similar to the one of Fernández et al. (2004), we find some differences in the distributions of elements upon entry. Figure 8 presents the distributions of perihelion distances (or rather peribaryon due to the use of barycentric reference frame) of bodies that reached an inner Oort Cloud starting at  $a = 10000$  AU – the initial distribution on the upper graph and the distribution at the moment of entry on the lower graph.

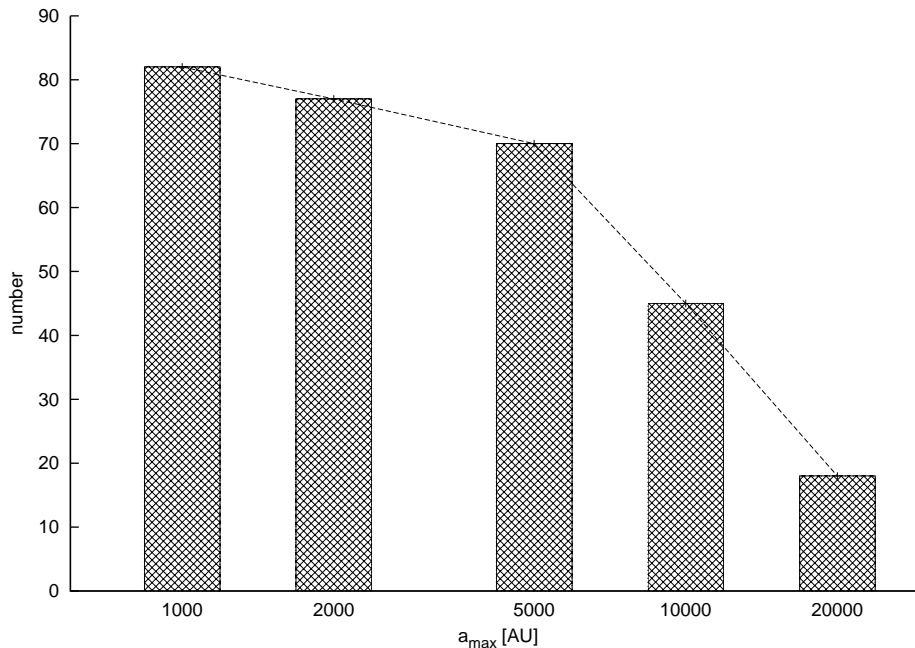


Fig. 7. Histogram of semi-major axis maximum values (plotted on a log scale) for our sample of SDOs.

The graphs are mutually similar, indicating very weak variations of the peribaryon distances of SDOs on their way to the inner Oort Cloud.

Planetary perturbations change the orbital energies of SDOs very efficiently and transfer them into different Solar System regions, but their peribaryon distances are much less diffused outside Neptune's orbit. This is characteristic of low-inclination evolution within the CR3BP. But as the lower panel shows, objects with perihelion/peribaryon distance over 36 AU can enter the inner Oort Cloud due to sole planetary perturbations within a 2 Gyr timescale. Even if we convert the values to the heliocentric reference frame, we get statistically the same result. Fernández et al. (2004) did not obtain this even after their 5 Gyr simulation. However, they did get more transfers caused by Jupiter, Saturn and Uranus than we did. We may view this as an independent confirmation of the effect they called Neptune's dynamical barrier, favoring outward evolution over the other end states.

It is hard to compare our results with the ones of Leto et al. (2009) due to differences of the Solar System model and the definition of the inner Oort Cloud region. Leto et al. started their integrations from quasi-circular orbits in the protoplanetary disk with the inclusion of perturbations due to the giant planets, the Galactic tides and stellar encounters. They assumed that an object reached the Oort Cloud, when  $q > 50$  AU and  $2000 < a < 25000$  AU. In the presence of such large differences, no correspondence of outcomes should be expected.

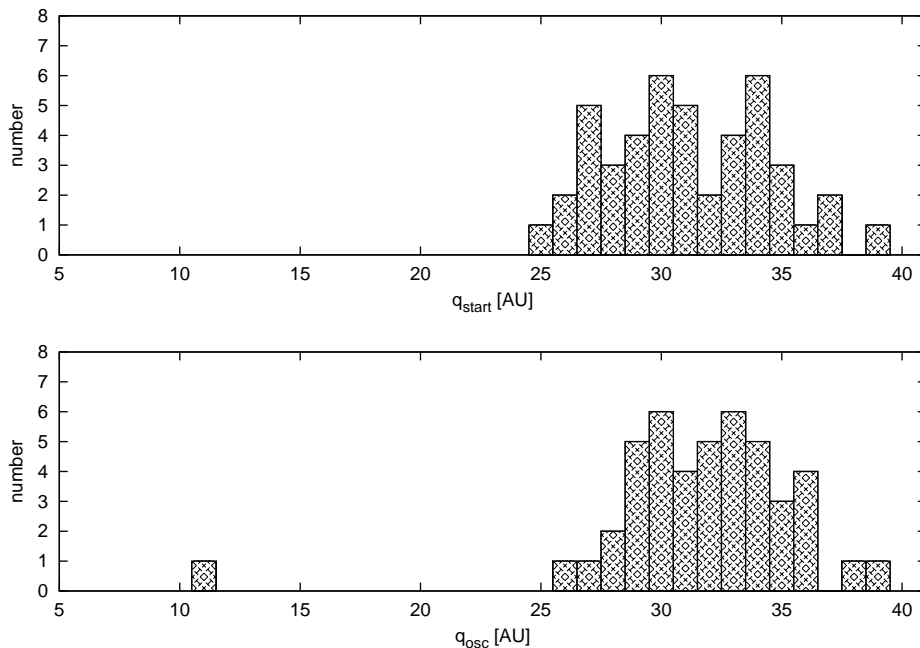


Fig. 8. Number of SDOs reaching the inner Oort Cloud (assumed to start at  $a = 10000$  AU) as a function of starting peribaryon distance (upper graph) and osculating peribaryon distance at the time of entry (lower graph).

#### 4. Conclusions

Conclusions from the results can be summarized as follows:

- Planetary perturbations are able to significantly change the orbital energies of SDOs, even if these are detached from the planetary system. The perihelion distance of the objects reaching inner Oort Cloud may remain quasi-constant on dynamically long timescales. The influence of very slow variations of the argument of periapsis via differential  $1/a$  perturbations is far too small to explain the observed large changes in semi-major axis for low-inclined particles.
- The influence of  $\omega$ -related differential  $1/a$  perturbations depends on the inclinations of the orbits. The larger the inclination of an orbit, the larger these perturbation become, with a maximum over  $i \simeq 40^\circ$ . The largest value of differential  $1/a$  perturbations are found for  $\omega \simeq 30 - 40^\circ$  in absolute value.
- The Kozai resonance does not seem to be a very efficient mechanism of increasing perihelion distances, unless it is associated to a MMR.
- Diffusion of perihelion distances of SDOs is low during 2 Gyr evolution outside Neptune's orbit. But objects with perihelion/peribaryon distances

larger than 36 AU are able to enter the inner Oort Cloud region within this timescale.

- As noted by Fernández et al. (2004), SDOs can be perceived as a source of feeding the inner Oort Cloud population. Our results indicate that large fractions of SDOs with perihelia in the range out to at least  $\sim 35$  AU do enter at least temporarily into the semi-major axis range of the inner Oort Cloud. They may form the basis of simulation techniques, whereby we may efficiently investigate the outcomes of including the Galactic tides and stellar encounters. Thus we may in the future be able to check the efficiency of actual feeding, as estimated by previous authors (e.g., Leto et al. 2009), by removal of the perihelia beyond the range where the planets act.

**Acknowledgements.** We thank the referee for helpful comments that improved the manuscript. This work was supported by the MNII grant N N203 392 734.

#### REFERENCES

- Chambers, J. E. 1999, *MNRAS*, **304**, 793.  
Duncan, M. J., Quinn, T., Tremaine, S. 1987, *AJ*, **94**, 1330.  
Duncan, M. J., Levison, H. F. 1997, *Science*, **276**, 1670.  
Fernández, J. A., Gallardo, T., Brunini, A. 2004, *Icarus*, **172**, 372.  
Gallardo, T. 2006, *Icarus*, **181**, 205.  
Gomes, R. S., Gallardo, T., Fernández, J. A., Brunini, A. 2005, *CM&DA*, **91**, 109.  
Leto, G., Jakubik, M., Paulech, T., Neslušan, L., Dybczyński, P. A. 2009, *EMP*, **105**, 263.  
Luu, J., Marsden, B. G., Jewitt, D., Trujillo, C. A., Hergenrother, C. W., Chen, J., Offutt, W. B. 1997, *Nature*, **387**, 573.  
Morbidelli, A., Brown, M. E. 2004, in “Comets II”, M. C. Festou, H. U. Keller and H. A. Weaver (Eds.), , 175.  
Rickman, H., Froeschlé, Ch., Froeschlé, Cl., Valsecchi, G. B. 2004, *Astro.&Astroph.*, **428**, 673.  
Rickman, H. 2010, in “Dynamics of Small Solar System Bodies and Exoplanets” by J. Souchay and R. Dvorak (Eds.), *Lecture Notes in Physics*, **790**, 341.  
Sitarski, G. 2002, *Acta Astron.*, **52**, 471.